Computational Study of KNI-272, a Potent Inhibitor of HIV-1 Protease: On the Mechanism of Preorganization

Laurent David,[†] Ray Luo,[†] Martha S. Head,[‡] and Michael K. Gilson*[,†,§]

Center for Advanced Research in Biotechnology, 9600 Gudelsky Drive, Rockville, Maryland 20850, National Institute of Standards and Technology, Gaithersburg, Maryland 20899, and SmithKline Beecham Pharmaceuticals, UW 2950, 709 Swedeland Road, P.O. Box 1539, King of Prussia, Pennsylvania 19406-0939

Received: September 10, 1998

The compound KNI-272 is a potent, peptide-like inhibitor of HIV protease. Its conformation when complexed with the protease is close to that which it assumes in its single-molecule crystal. This observation led to the suggestion that KNI-272 gains affinity by being preorganized for binding. On the other hand, one might well expect KNI-272 to be flexible because it possesses 15 rotatable bonds. Moreover, a recent ab initio study of KNI-272 suggests that it is not preorganized because its bound conformation is strained. Here, we use a novel algorithm to study the conformational distribution of this inhibitor. The results show good agreement with a recent NMR analysis of KNI-272 in solution. The calculations indicate that KNI-272 in solution occupies three major conformations, one of which matches the bound conformation and the NMR structure. In addition, the thioproline amide bond tends to be in the trans conformation found in the complex of KNI-272 with HIV protease. Further calculations on hypothetical analogues of KNI-272 provide information on the mechanism of preorganization and indicate that steric interactions among the bulky side chains are of particular importance.

1. Introduction

The compound KNI-272[1] is a potent inhibitor of the wild-type protease of human immunodeficiency virus 1 (HIV-1 PR). The dissociation constant of its complex with HIV-1 PR is a few picomoles per liter.[2] Chemically, KNI-272 resembles a pentapeptide with bulky, nonnatural side-chains, as illustrated in Figure 1a. The central allophenylnorstatine (Apns) residue possesses a backbone hydroxyl group that donates a hydrogen bond to Asp 125 of HIV-1 PR[3] and is thus believed to mimic the substrate transition state. The thioproline (Thp) residue that follows the Apns is an analogue of the proline residue found in the naturally occurring substrates of HIV-1 PR.

One might expect KNI-272 to be quite flexible, in the manner of many short peptides;[4,5] however, when the structure of the complex of KNI-272 with HIV-1 PR was solved,[3] its conformation proved to be similar to its conformation in the solid state. It was therefore conjectured that this molecule possesses an intrinsic tendency to adopt the conformation found in the complex with HIV-1 PR, i.e., that KNI-272 is preorganized into its active conformation. If this is correct, preorganization might be partly responsible for the high affinity of this inhibitor for its protein target.[3] A subsequent nuclear magnetic resonance (NMR) study[6] addressed this issue by examining the conformational preferences of KNI-272 in dimethyl sulfoxide (DMSO). The chief solution conformation that was identified is similar to the crystal conformations of KNI-272 (see above), and it was therefore concluded that KNI-272 is indeed significantly preorganized for binding.

On the other hand, a quantum chemical study of KNI-272[7] concluded that its bound conformation is strained. In particular, calculations on a small molecule that models the central Apns−Thp region suggested that one dihedral angle (T1 = ψ_{Thp}) is strained by 8−13 kJ/mol in the crystal conformation of KNI-272. It was also argued that the Apns−Thp amide bond has no intrinsic preference for the trans conformer found in the complex with HIV-1 PR and thus that this part of the molecule also is not preorganized.

Thus, there is still discussion regarding the degree to which KNI-272 is preorganized for binding to HIV-1 PR. In addition, the physical interactions that govern the conformational preferences of this peptide-like molecule are not fully understood. These issues are of considerable interest. For one thing, understanding the physical basis for the high potency of KNI-272 may be useful in developing this class of inhibitors as drug candidates. In addition, any lessons learned about the physical basis for preorganization in KNI-272 can be expected to apply more generally and thus to be useful in the development of compounds active against drug targets other than HIV-1 PR.

Here, we address these issues by computationally analyzing the conformational preferences of KNI-272 and comparing the results with the NMR and quantum chemical analyses discussed above. The conformational analysis is then repeated with modified energy models and with analogues of KNI-272 in order to study the forces that determine the conformational preferences of this inhibitor. The calculations use a novel and highly efficient algorithm[8] for mapping the energy minima of a flexible molecule. This algorithm also quantifies the free energy associated with each energy minimum and thus yields the relative populations of the various conformations. Previous applications of this method to the calculation of small-molecule pK_a shifts,[9] ion pairing in aqueous solution,[10] and the binding affinities of small molecules in chloroform[11] have yielded good agreement with experiment.

The paper is organized as follows. The Methods section begins by reviewing the experimental data obtained in the NMR study. This provides a defined basis for the subsequent

* Corresponding author. E-mail: gilson@indigo14.carb.nist.gov.
† Center for Advanced Research in Biotechnology.
‡ SmithKline Beecham Pharmaceuticals.
§ National Institute of Standards and Technology.

10.1021/jp983675l CCC: $18.00
Published on Web 01/20/1999

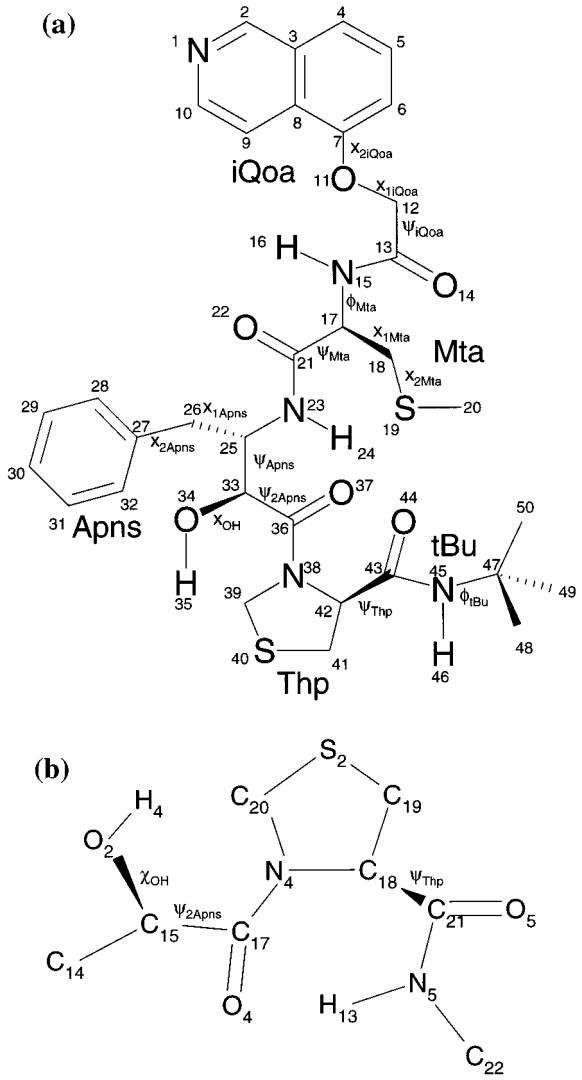

Figure 1. (a) Structure of KNI-272. (b) Structure of small-molecule fragment of KNI-272, compound 4 from Murcko et al.[7]

comparison between computation and experiment. The computational methodology is then presented. The Results and Discussion section first describes the computed conformational distribution of KNI-272 in solution. The degree of preorganization is assessed by comparison with the conformation of KNI-272 in its complex with HIV-1 PR. Then, the factors that control the conformation of KNI-272 are analyzed by further calculations on analogues of KNI-272. In addition, the differences between the present results and those of the previous computational study of KNI-272 are examined. Particular attention is given to the possibility of strain in the Apns−Thp region, which was a focus of the previous study. The Results and Discussion section concludes with an extensive comparison of the computational results with the previously reported NMR results. The generally good agreement with experiment justifies the use of the present computational method to study the preorganization of KNI-272. The Conclusions section briefly states the chief results of this study.

2. Methods

2.1. Review of the Experimental Data. The conformational distribution of KNI-272 in dimethylsulfoxide (DMSO) has been studied by NMR.[6] The study yielded 29 nuclear Overhauser effect (NOE) distance constraints, and 6 coupling constants that provided limited information about 3 torsion angles. The NOEs

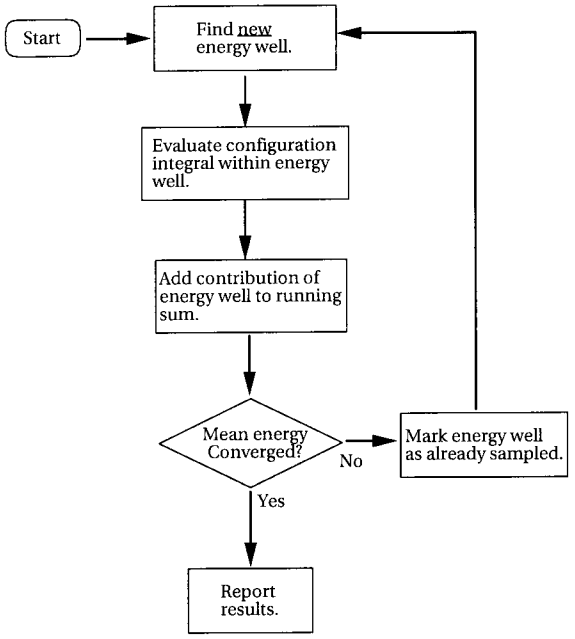

Figure 2. Flowchart of the mining minima algorithm.

were categorized as "weak", "medium", and "strong"; these categories were taken to imply interproton distances of less than 4.5, 3.5, and 2.5 Å, respectively. These distance limitations were then used as restraints in a simulated annealing protocol (applied on pseudoatom distances[12]) that yielded three main conformers designated A, B, and C. As shown in Table 4 of this paper, the conformers differ chiefly in one dihedral angle, ψ_{Apns}. Three other dihedral angles also differ, but these have little effect on the overall shape of KNI-272 because they are near its termini. This variability may reflect a lack of distance information around the Cα and Cβ of this residue. However, the HMBC spectrum suggests that this dihedral angle is likely to be in the trans form,[6] which corresponds to conformation A.

The Thp residue possesses a cyclic side chain like that of proline. As a consequence, the probability that the Apns−Thp amide bond occupies a cis conformation is increased relative to a normal, noncyclic residue.[13] However, a ROESY analysis indicated that this angle is predominantly trans, with a trans/cis ratio of 5.7, and only the trans conformation was included in the conformational analysis. As a consequence, conformations A, B, and C all have this angle in the trans form, and our conformational analysis accordingly assumes this conformation also. However, a separate calculation of the trans/cis ratio of the amide was done for comparison with the result of the ROESY study.

2.2. Calculation of Conformational Distributions. *2.2.1. "Mining Minima" Algorithm.* The "Mining Minima" (MM) algorithm[8] is used to locate the low-energy conformations of KNI-272 and to compute their stabilities. This algorithm, diagrammed in Figure 2, proceeds as follows. First, a new minimum-energy structure is identified via a rapid optimization method that has been described previously.[8] Next, the extent of the potential energy well associated with the current energy minimum is determined and the free energy (configuration integral) of that minimum is computed by Monte Carlo integration of the Boltzmann factor. The contribution of this well is added to a running sum of the free energy. If adding this contribution produces a significant change in the overall free energy, the calculation is not converged; the current energy well is marked as already included in the sum, and the algorithms cycles back to find a new energy well. If the sum is

converged, then the calculation stops and the free energy is reported. The energy-minimum conformations found by this procedure are stored along with their associated free energies. Within each energy well, Monte Carlo integration continues until the result converges to a fractional change of $<10^{-4}$. New energy wells are included until their contributions to the free energy drop to a fractional change of $<10^{-6}$. Bond lengths and bond angles are treated as fixed during sampling in the present implementation. The calculations are carried out with a local version[8,9] of the program UHBD.[14]

To check for numerical convergence, MM calculations were carried out with two different starting conformations of KNI-272, i.e., with different initial dihedral angles. These yielded total free energies that agreed to within 0.3% and also yielded the same clusters of low-energy conformations (see below).

2.2.2. Energy Model. The energy as a function of molecular conformation may be separated into a vacuum energy term and a solvation term.[15] The vacuum energy is computed here with the CHARMM22 parameter set[16] with the all-hydrogen representation (see Molecular Models section). The solvation energy may be estimated with the generalized Born/surface area (GB/SA) model,[17] which is a rapid approximation to the Poisson−Boltzmann/surface tension model.[18] These models estimate the solvation energy by separating the process of solvation into two hypothetical steps, formation in the solvent of a Lennard-Jones cavity having the shape of the solute (nonpolar solvation) and electrostatic charging of the atomic partial charges within the cavity (electrostatic solvation).

The cavity radius assigned to each non-hydrogen atom of KNI-272 is similar to the van der Waals radius (R_{min}) appropriate to its CHARMM22 atom type. The actual cavity radius used is the average of R_{min} and 1.4 Å. A previous study[9] showed that this adjustment yields better agreement with experiment for solvation free energies. Hydrogen radii were set to 1.2 Å.[9] The solute dielectric constant was set to 1, and the solvent dielectric constant was set to 45 for DMSO or 80 for water.

We examined the contribution of the surface area term to the variation in the solvation energy of KNI-272 as a function of conformation as follows. The MM method was used to find the low-energy conformations of KNI-272 with GB electrostatics[19] alone and with the full GB/SA model. The surface area coefficient was set to a value appropriate to water, 25.1 J/(mole Å^2).[20,21] Probe−center surface areas were computed by a rapid algorithm[22] with a probe of radius 1.4 Å. The two sets of energy minima that resulted from the GB and GB/SA calculations were very similar to each other. In addition, the variation in the surface area-dependent energy was very small; the surface energies of the minima generated with GB/SA ranged over only 0.75 kJ/mol (0.3kT). For comparison, the range of the electrostatic part of the solvation energy was 3.1 kJ/mol. The importance of the surface area term was examined further by varying the angle $\psi_{2,Apns}$ and thus forming or breaking a hydrophobic contact between the *t*-Bu and Apns side chains. This change altered the surface area by only about 10 Å^2, which corresponds to the negligible energy change of 0.25 kJ/mol or about 0.1kT. On the basis of this analysis, the surface area part of the GB/SA model was omitted, and solvation energies were computed with only the GB electrostatic term.[17]

2.2.3. Molecular Models. KNI-272. KNI-272 is a pentapeptide-like molecule (see Figure 1a) with the following sequence of residues: 5-isoquinolyloxyacetyl (iQoa), methylthioalanine (Mta), allophenylnorstatine (Apns), thioproline (Thp), tertiary butylamine (*t*-Bu). Except as otherwise noted, calculations for KNI-272 and its variants have the Apns−Thp peptide bond in the trans conformation. This is appropriate because the trans conformer predominates in solution and is the focus of the NMR conformational study (see above). The starting conformation for KNI-272 was taken from PDB entry 1hpx[3] with all hydrogen atoms deleted. The molecular editor of the Quanta package[23] was used to create the topology of the molecule. All hydrogen atoms were added, and the atom types were assigned automatically. Most of the atoms are readily identified as similar to ones in the standard 20 amino acids. However, it is worth noting that both sulfur atoms were assigned atom type SE (thioether sulfur) and that the oxygen of the iQoa residue was assigned atom type OE (ether/acetal oxygen). The complete list of atom types is given in Table 1. Atomic charges were also assigned automatically in Quanta, using the CHARMM22 template charges. The total charge of the molecule was set to 0 using the smoothing function over the nonpolar atoms. The sulfur atoms in the CHARMM22 force field are represented by a point charge; no lone pairs are used. The atomic partial charges also are listed in Table 1. With the GB solvation model, 2000 steps of steepest descent energy minimization were carried out using an internal dielectric of 1 and an external dielectric of 45 to simulate the dimethylsulfoxide used in the NMR experiment.[6]

TABLE 1: QUANTA/CHARMM Atom Types and Atomic Point Charges (Elementary Charges)[a]

no.	type	charge	no.	type	charge	no.	type	charge
1	N6R	−0.540	2	C6R	−0.125	3	CR66	0.000
4	C6R	−0.125	5	C6R	−0.125	6	C6R	−0.125
7	C6R	0.255	8	CR66	0.000	9	C6R	−0.125
10	C6R	0.255	11	OE	−0.230	12	CT	0.096
13	C	0.600	14	O	−0.550	15	NP	−0.400
16	H	0.250	17	CT	0.056	18	CT	−0.044
19	SE	−0.100	20	CT	−0.094	21	C	0.600
22	O	−0.550	23	NP	−0.400	24	H	0.250
25	CT	−0.094	26	CT	−0.094	27	C6R	0.006
28	C6R	−0.125	29	C6R	−0.125	30	C6R	−0.125
31	C6R	−0.125	32	C6R	−0.125	33	CT	−0.094
34	OT	−0.650	35	HO	0.400	36	C	0.600
37	O	−0.550	38	NX	−0.250	39	CT	0.096
40	SE	−0.100	41	CT	−0.044	42	CT	0.056
43	C	0.600	44	O	−0.550	45	NP	−0.400
46	H	0.250	47	CT	−0.094	48	CT	−0.094
49	CT	−0.094	50	CT	−0.094			

[a] The nonpolar hydrogens are all of type HA. The aromatic hydrogens have a charge of 0.135 and hydrogens bonded to methyl or methylene have a charge of 0.056, except for the hydrogen of Apns Cα, which has a charge of 0.105.

The MM calculations varied 15 rotatable dihedral angles (see Figure 1a): ψ_{iQoa}, χ_{iQoa}, $\chi_{2,iQoa}$, ϕ_{Mta}, ψ_{Mta}, χ_{Mta}, $\chi_{2,Mta}$, ϕ_{Apns}, ψ_{Apns}, $\psi_{2,Apns}$, χ_{Apns}, $\chi_{2,Apns}$, ψ_{Thp}, ϕ_{t-Bu}, and $\chi_{OH,Apns}$ (the hydroxyl of the Apns main chain). The ϕ and χ angles of Thp were kept rigid. The validity of this simplification is supported by a molecular dynamics simulation of KNI-272 with the GB solvation model (data not shown). The simulation yielded a mean value of −67.9° for ϕ_{Thp}, with a standard deviation of 13.2°, and the mean χ_{1-4} angles of the ring were 9.5°, −5.3°, −0.6°, and 6.9°, respectively. The corresponding standard deviations were 25°, 27.6°, 23.2°, and 16.4°. For comparison, the values of these angles in the complex with HIV-1 PR are −66.0°, 21.7°, −20.1°, 12.8°, and −1.4°, respectively. Thus, with this force field, the ring remains nearly planar with minor fluctuations, justifying the approximation that its conformation is fixed. It is also worth noting that the conformation of this ring changes minimally on going from single-crystal structures to the complex with HIV-1 PR.[3] The methyl groups of *t*-Bu and Mta were not allowed to rotate. This simplifies the calculation and has little effect on the results. For example,

repeating the MM computation with the Mta methyl torsion included as rotatable changed the cumulative free energy by only 0.24%.

The sensitivity of the calculations to the bond lengths and bond angles of KNI-272 was examined by repeating the MM calculations with a different starting conformation. This conformation was generated by resetting the main-chain torsion angles of KNI-272 to arbitrary values ($\psi_{iQoa} = 101°$, $\phi_{Mta} = -169°$, $\psi_{Mta} = -84°$, $\phi_{Apns} = -47°$, $\psi_{Apns} = 89°$, $\psi_{2,Apns} = -145°$, $\psi_{Thp} = -13°$) and energy-minimizing with the conjugate-gradient method in Quanta. The energy minimization ran for 5000 steps and yielded a final root-mean-square atomic force of 0.06 kJ/mol/Å. The dielectric constant was fixed at 50 in order to prevent structural distortions from strong in vacuo Coulombic interactions. This procedure yielded a conformation with altered bond lengths and bond angles. The MM calculations were then repeated with this new conformation. As noted in Results, this change in the starting conformation produced little change in the computed conformational distribution.

In section 3.3.3., we compute the trans/cis ratio of the Apns−Thp peptide bond. This ratio is given by $\exp[-(A_{trans}-A_{cis})/RT]$, where A_{trans} and A_{cis} are the conformational free energies of the KNI-272 in the trans and cis conformations, respectively. Computing these quantities requires that the MM procedure be run once with the trans conformation and again with the cis conformation. The initial trans structure used in these MM calculations was prepared as described above, followed by an additional 5000 steps of steepest descent energy minimization with a dielectric constant of 50. The initial cis structure was prepared by rotating the peptide angle to 180° and energy-minimizing in the same way. Extensive energy minimization is needed so the free energy differences between the two ensembles of conformations generated by the MM method will be rigorously comparable.

Analogues of KNI-272. To study the basis of preorganization in KNI-272, MM calculations were carried out for computationally generated analogues of KNI-272 (see Table 5 and section 3.2). The structures for these were created with Quanta based on the initial conformation of wild-type KNI-272. After each modification was made, 200 steps of steepest-descent energy minimization were carried out in Quanta, with a dielectric constant of 50. This high value weakens electrostatic contributions (as does GB) and allows the bond lengths and angles to be relaxed following the changes to KNI-272.

Small Molecule Fragment of KNI-272. Calculations were also carried out for a small molecule (Figure 1b) that models the most rigid part of KNI-272 (see below). This is the same as compound 4 of Murcko and co-workers.[7] The compound was created in Quanta by deleting the appropriate atoms from the starting conformation of KNI-272 and adding back hydrogens to preserve valence. To test for sensitivity to bond lengths and angles, these calculations were repeated with the alternate starting structure of KNI-272 described above.

NMR Conformations. The three conformations of KNI-272 identified in the NMR study of Ohno et al.[6] were constructed for comparison with our computationally generated structures. The NMR conformations were constructed from the crystal conformation in 1hpx by rotating the dihedral angles to the values given by Ohno et al. (Table 4). Then, the structures were energy-minimized with a constraint of 0.5 J/degree^2 on each of the 10 dihedral angles whose value was specified in the NMR study. This minimization used 300 steps of the Broyden−Fletcher−Goldfarb−Shanno method (BFGS)[24] as implemented in UHBD with an internal dielectric of 1. (Screening the electrostatic forces is not necessary here because of the dihedral constraints.) Note that the NMR study did not yield values for every rotatable bond.

2.3. Conformational Analysis. *2.3.1. Clustering of Conformations.* The low-energy conformations generated by the MM method were clustered according to the root-mean-square deviations (RMSDs) of cartesian coordinates of subsets of atoms. Clustering was based either upon the coordinates all main-chain atoms, or upon all main-chain atoms except those in iQoa and Mta, as detailed in Results. For each pair of conformations, the Kabsch method[25] was used to optimize the superposition of the selected atoms and the resulting RMSD was computed. If this RMSD was less than 0.5 Å, the two conformations were included in the same cluster. Each cluster was extended to include all conformations having an optimized RMSD within 0.5 Å of any other conformation in the cluster. Note that a cluster can contain two conformations with an RMSD greater than 0.5 Å if both conformations have an RMSD less than 0.5 Å relative to a third conformation.

The free energy $G_{c,i}$ associated with each cluster i was then calculated as follows:

$$G_{c,i} = -RT \ln \sum_{j=1}^{N_i} \exp(-G_j/RT) \tag{1}$$

where N_i is the number of conformations in cluster i and G_j is the free energy of conformation j. It is worth emphasizing that the MM method does not double-count conformations; the algorithm never generates a given conformation more than once. The probability P_i that the conformation of KNI-272 lies within cluster i is then given by

$$P_i = \frac{\exp(-G_{c,i}/RT)}{\sum_{k=1}^{N_c} \exp(-G_{c,k}/RT)} \tag{2}$$

where N_c is the number of clusters.

Each cluster can be characterized by its mean dihedral angles. The mean value of dihedral angle ϕ for cluster i is

$$\langle\phi_i\rangle = \frac{\sum_{j=1}^{N_i} \phi_j \exp(-G_j/RT)}{\sum_{j=1}^{N_i} \exp(-G_j/RT)} \tag{3}$$

where ϕ_j is the value of ϕ for conformation j.

The probability distribution of each dihedral angle is computed without reference to the clusters. Thus, the probability that angle ϕ lies in the range $[\alpha, \alpha + 5°]$ is given by

$$P(\phi,\alpha) = \frac{\sum_{j=1}^{N} \chi_{\phi,\alpha,j} \exp(-G_j/RT)}{\sum_{j=1}^{N} \exp(-\mathrm{Gj/RT})} \tag{4}$$

where $\chi_{\phi,\alpha,j}$ equals 1 if $\phi_j \in [\alpha,\alpha + 5°]$ and 0 otherwise, and N is the total number of energy minima in all clusters.

2.3.2. Mean Interproton Distances. Mean interproton distances were computed to provide a relatively direct comparison (section 3.3.2) with the NOE data for KNI-272.[6] An NOE

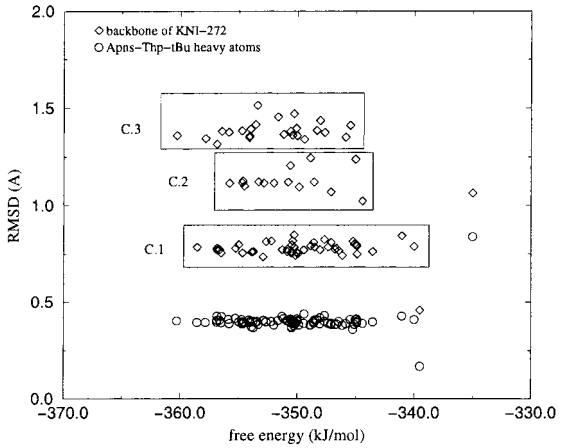

Figure 3. Free energies (kJ/mol) of KNI-272 for the energy minima given by the mining minima procedure plotted against their RMSD values (Å) relative to the C.A NMR conformer[6].

interaction depends on the interproton distance as r^{-6}, so the average distances must be weighted accordingly. Thus, the mean distance between protons a and b is computed as

$$\langle r_{ab}\rangle = \left(\frac{\sum_{j=1}^{N} r_{ab,j}^{-6} \exp(-G_j/RT)}{\sum_{j=1}^{N} \exp(-G_j/RT)} \right)^{-1/6} \quad (5)$$

where $r_{ab,j}$ is the distance between protons a and b for conformation j.

The experimental NOEs for KNI-272 do not distinguish between chemically symmetric protons, such as those of a methyl group or the β carbon of an amino acid. In such cases, we compute a mean interproton distance that is an average over the equivalent protons. Thus, if an NOE corresponds to the interaction of one set of n equivalent protons with another set of m equivalent protons (e.g., methyl with β carbon), the mean distance is computed as

$$\left(\frac{1}{nm} \sum_{a}^{n} \sum_{b}^{m} \langle r_{ab}\rangle^{-6} \right)^{-1/6} \quad (6)$$

3. Results and Discussion

This section first describes the conformations of KNI-272 generated by the computational methodology described above. Perhaps the most striking result is that the C-terminal residues of KNI-272 are preorganized into the active inhibitory conformation found in the complex with HIV-1 PR. Further calculations indicate that the preorganization of the C-terminal residues depends on a limited set of specific steric and electrostatic interactions. Comparisons with the NMR study of KNI-272 in DMSO show good agreement with the experimental structures and NOEs. Good agreement also is found for the trans/cis ratio of the proline-like amide bond at Thp.

3.1. Conformational Analysis of KNI-272: Clustering and Preorganization. The mining minima calculation for KNI-272 in DMSO converged when 88 low-energy conformations had been generated. The probability distribution of each dihedral angle (eq 4) is illustrated in Figure 6a. The distribution of conformations is illustrated differently in Figure 3, which plots the free energy G_j of each conformation relative to the RMSD computed relative to the "A" conformer of Ohno et al. (These RMSDs were computed with main-chain atoms only.) Clustering of the conformations according to their main-chain RMSDs (see Methods) yields the three clusters C1, C2, and C3 that are marked in the Figure 3 (diamonds). The free energies $G_{c,i}$ and probabilities P_i of the three clusters, computed with eqs 1 and 2, are listed in Table 2. Clusters C1 and C3 each have probabilities of 40−50%, while C2 is about 10% occupied. The spread of main-chain conformations within each cluster is small; the main-chain RMSD values found within each cluster are 0.75 Å or less. As shown in Table 3, the differences between the clusters are larger, 1−2 Å.

TABLE 2: Characteristics of Each Cluster: Free Energy (kJ/mol), Occupancy, and Maximum Root-Mean-Square Deviation (RMSD) (Å) between Main-Chain Atoms for Any Pair of Structures within Each Cluster

	cluster		
	C.1	C.2	C.3
free energy (kJ/mol)	−361.96	−358.82	−362.30
% occupancy	41.6	10.6	47.8
maximum RMSD within cluster	0.76	0.28	0.52

TABLE 3: Comparison of Various Conformations of KNI-272 after Least-Squares Alignment of Selected Atoms[a]

	calculated			NMR		
	C.1	C.2	C.3	C.A	C.B	C.C
C.X	0.4/0.4	1.2/0.4	1.4/0.4	0.5/0.4	2.0/1.8	1.7/1.2
C.1		1.0/0.0	1.6/0.1	0.6/0.4	1.8/1.8	1.9/1.3
C.2			1.8/0.1	1.2/0.4	1.6/1.8	1.6/1.3
C.3				1.5/0.4	2.4/1.8	1.9/1.3
C.A					2.0/1.9	1.7/1.3
C.B						1.9/2.1

[a] C.1, C.2, C.3: lowest-energy representative of each computed cluster. CX: crystal structure with HIV-1 PR.[3] C.A, C.B, C.C: NMR structures;[6] C.A was deemed the most probable.[6] Numbers before the slash are RMSD values (Å) for the 18 main-chain atoms; numbers after the slash are for all atoms in the C-terminal residues Apns, Thp, and *t*-Bu.

Figure 4 shows two views of the lowest-energy conformations generated by the MM procedure. These include representatives of each cluster. The structures are oriented to optimize the superposition of the C-terminal residues Apns, Thp, and *t*-Bu. It is evident that the C-terminal conformations are very similar but that there is significant variation in the N-terminal residues iQoa and Mta. The variations are examined in more detail in Table 4, which provides the mean and standard deviation of the dihedral angles for each cluster (eq 3). The chief difference between the clusters is in the ϕ angle of one of the N-terminal residues, Mta. In addition, the ψ angle of the N-terminal iQoa residue has particularly large standard deviations indicating a high degree of flexibility. The other dihedral angles, especially those in the C-terminal residues, are remarkably constant. As a consequence, reclustering the 88 conformations of KNI-272 according to the main-chain RMSDs of only the C-terminal residues Apns, Thp, and *t*-Bu causes all the conformations to fall into a single cluster. This is illustrated in the plot of free energy against RMSD computed for only the C-terminal atoms (circles in Figure 3).

If KNI-272 is preorganized for binding to HIV-1 PR, then its conformations in solution should overlap with the conformation adopted in its complex with HIV-1 PR. Figure 5 shows that the lowest-energy conformations in cluster C1 do strongly resemble the conformation of bound KNI-272. Thus, the main-chain atoms of the lowest-energy member of cluster C1 deviate from the crystal conformation by only 0.4 Å (Table 3) and the deviation of all non-hydrogen atoms is 0.89 Å. Moreover, all

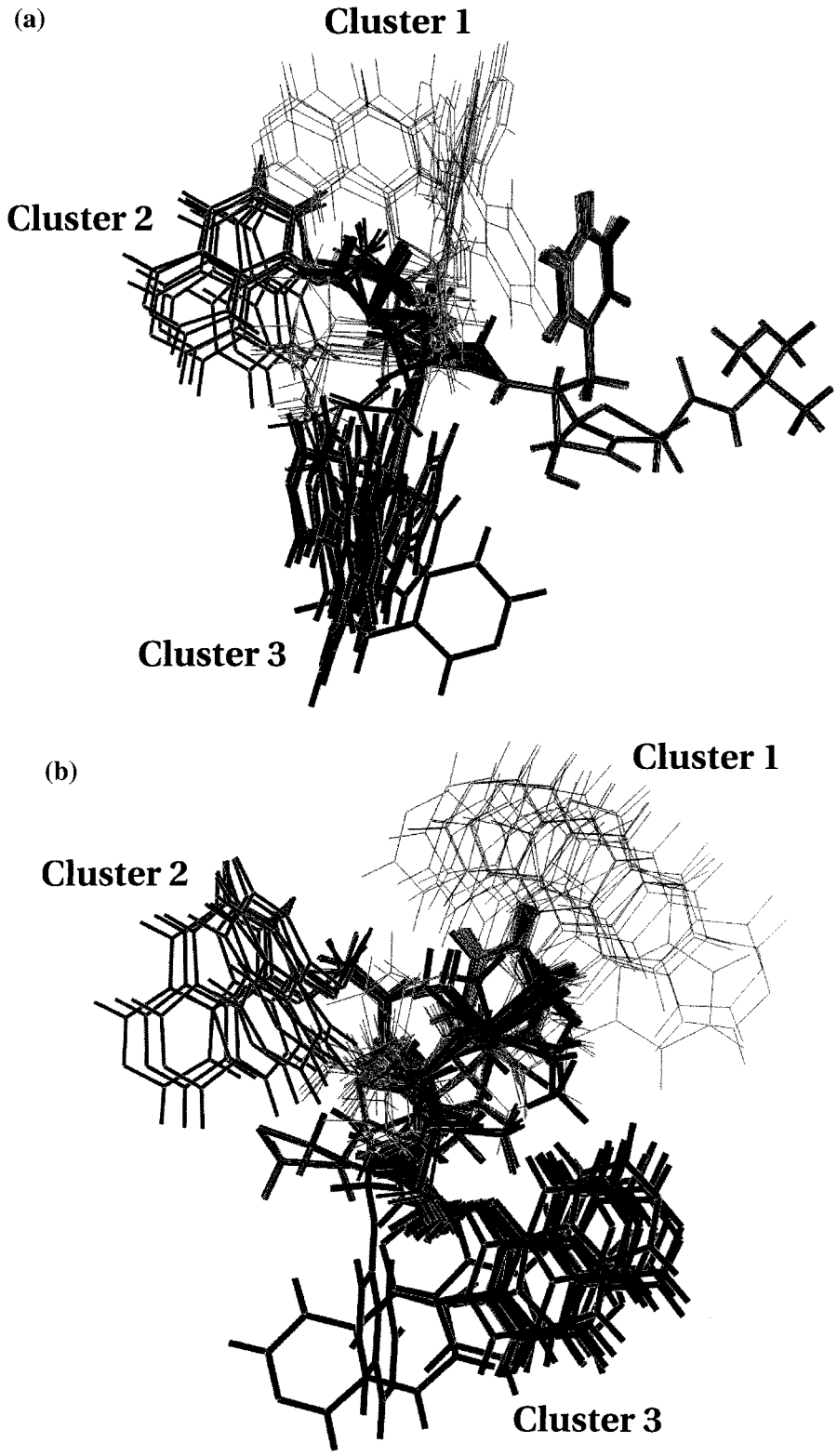

Figure 4. Overlay of the 33 low-energy conformations whose energy is within 9 kJ/mol of the global energy minimum. The clusters are identified as follows: (thin line) C.1; (medium line) C.2; (thick line) C.3. The two views are related by a 90° rotation around the vertical axis.

three clusters of conformations resemble the crystal conformation in their C-terminal portion; the deviations are only 0.4 Å (Table 3). Table 4 shows the similarity between the computed torsion angle distributions and the torsion angles found in the crystal structure. In summary, the present calculations suggest that KNI-272, and in particular its C-terminus, is preorganized into the conformation that binds HIV-1 PR.

The calculations just described use a starting conformation of KNI-272 that is based upon its conformation in the HIV-1 PR binding site. It was of concern that this might bias the calculated distribution of conformations. However, repeat calculations with the alternate starting conformation described in Methods produce extremely similar results. This may be seen by comparing the new dihedral distribution, shown in Figure

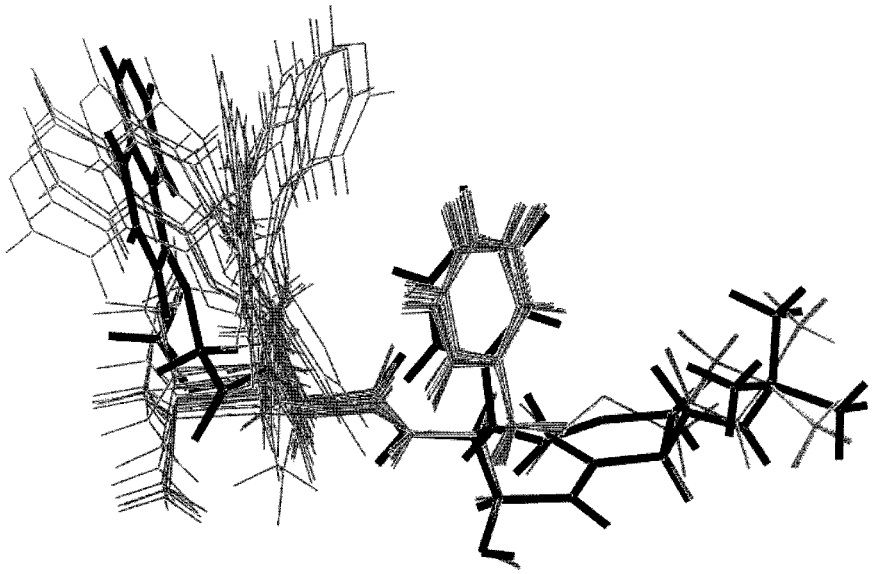

Figure 5. Overlay of the crystal conformation of KNI-272[3] (thick line) with the C.1 conformations within 9 kJ/mol of the global energy minimum (thin line).

TABLE 4: Dihedral Angles (degrees) of KNI-272[a]

	calculated							NMR		
	C.1		C.2		C.3					
angle	mean	SD	mean	SD	mean	SD	CX	C.A	C.B	C.C
iQoa ψ	−21.1	46.7	5.6	21.0	6.2	40.0	36.0	58.4	130.1	59.0
iQoa χ	−174.7	14.9	−178.8	2.6	177.9	1.8	−169.0	179.5	78.0	179.6
Mta ϕ	−88.3	5.2	−71.8	0.7	−68.6	1.1	−119.0	−145.4	−144.2	−145.1
Mta ψ	70.9	17.9	156.9	1.5	−39.1	1.7	74.0	80.1	84.9	79.4
Mta χ	−54.1	15.6	−55.5	0.5	−53.9	15.9	−166.0	−65.6	−65.9	−65.6
Apns ϕ	−95.8	13.3	−86.1	1.5	−106.1	5.5	−107.1	−111.2	−114.4	−110.8
Apns ψ	177.2	1.7	177.6	0.3	178.5	1.5	164.4	166.8	−58.7	71.9
Apns ψ_2	−83.9	0.5	−83.6	0.3	−83.9	0.2	−90.6	−73.3	−94.1	−92.9
Apns χ	−62.7	2.8	−63.6	0.5	−60.7	1.0	−56.4	−73.0	−66.9	−73.7
Thp ψ	118.3	1.0	119.2	0.4	118.6	0.6	146.8	138.4	−48.1	120.5

[a] C1, C2, and C3: calculated Boltzmann averages and standard deviations for the three clusters. CX: complexed with HIV-1 PR.[3] CA, CB, CC: the three NMR conformations,[6] built as described in Methods.

6b, with the original dihedral distribution in Figure 6a. In addition, the same three conformational clusters are obtained, and their relative probabilities are little changed; the new probabilities are 36.7%, 10.4%, and 52.8% for clusters C1, C2, and C3, respectively. Thus, the results do not depend significantly upon the choice of starting conformation.

These calculations are for the nonaqueous solvent DMSO. This permits direct comparison with the NMR study, which used this solvent. However, it is reasonable to ask whether KNI-272 will also be preorganized in water. We find that calculations with a solvent dielectric constant appropriate to water (80) instead of DMSO (45) yield essentially the same distribution of conformations. This is evident from a comparison of the dihedral density distributions computed for DMSO (Figure 6a) and water (Figure 6c).

3.2. Factors Contributing to the Preorganization of KNI-272. The calculations in the previous section suggest that KNI-272 and especially its C-terminal residues are strongly preorganized in solution. This section analyzes the factors that contribute to preorganization by examining the conformational distributions of analogues of KNI-272. First, three residues in turn are changed to glycines and the bulky *t*-Bu group is replaced by a methyl group. The conformational distribution is also recalculated with various treatments of electrostatic interactions and of the solvent. The conformational changes that result from these modifications are summarized in Table 5. Finally, further analysis is carried out for a small molecule representing the most rigid part of KNI-272.

3.2.1. Analogues of KNI-272. Thp → Gly. It would be reasonable to suppose that the proline-like Thp residue helps to preorganize KNI-272 by freezing the angle ϕ_{Thp}. The value of this angle is −65° in the computations described above. This idea was tested by changing Thp to a glycine (Gly), the amino acid that allows maximal flexibility of the main chain. Surprisingly, perhaps, this change has little effect on the conformational distribution of KNI-272. This is evident from a comparison of the dihedral distributions of the wild-type (Figure 6a) and the analogue (Figure 6d). The chief changes are as follows. Although ψ_{Gly} is still primarily at 120°, it now assumes a gauche$^-$ conformation with 2% probability. Similarly, ϕ_{Gly} still assumes the value of −75° with greater than 95% probability, but there is now a 4% probability of assuming a value of 85°. Thus, the proline-like ring of the Thp residue is not essential for the preorganization of KNI-272. In particular, the C-terminus is predicted to retain its original conformation when Thp is replaced by Gly.

t-Bu → Methyl. We hypothesized that steric and van der Waals interactions between the bulky *t*-Bu group and the phenyl ring of Apns might be responsible for constraining the conformation of KNI-272. This was tested by replacing the *t*-Bu group with a much smaller methyl group and repeating the conformational analysis. The resulting distribution of dihedral angles,

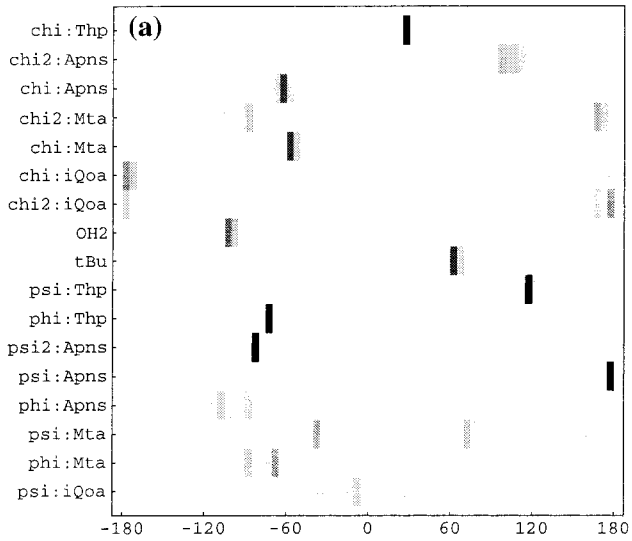
(a)
chi:Thp
chi2:Apns
chi:Apns
chi2:Mta
chi:Mta
chi:iQoa
chi2:iQoa
OH2
tBu
psi:Thp
phi:Thp
psi2:Apns
psi:Apns
phi:Apns
psi:Mta
phi:Mta
psi:iQoa
-180 -120 -60 0 60 120 180

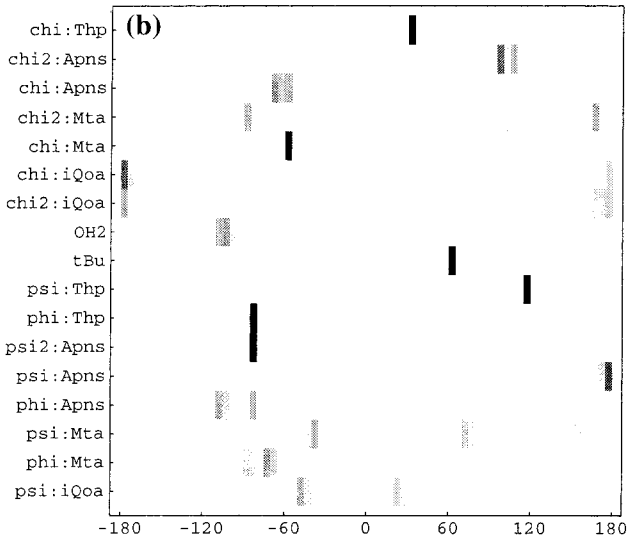
(b)
chi:Thp
chi2:Apns
chi:Apns
chi2:Mta
chi:Mta
chi:iQoa
chi2:iQoa
OH2
tBu
psi:Thp
phi:Thp
psi2:Apns
psi:Apns
phi:Apns
psi:Mta
phi:Mta
psi:iQoa
-180 -120 -60 0 60 120 180

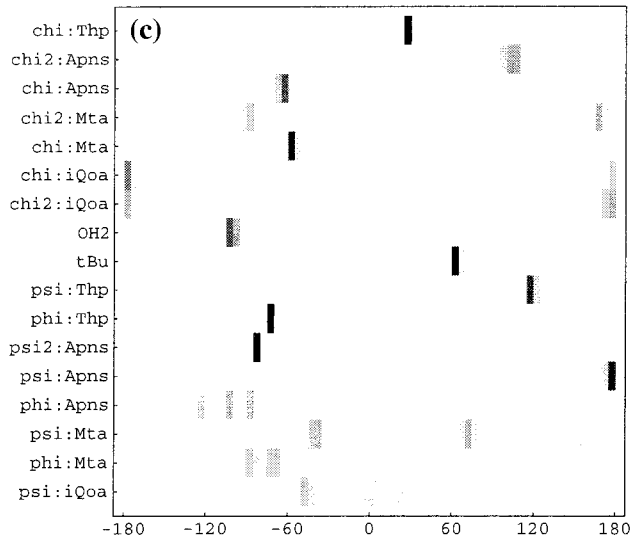
(c)
chi:Thp
chi2:Apns
chi:Apns
chi2:Mta
chi:Mta
chi:iQoa
chi2:iQoa
OH2
tBu
psi:Thp
phi:Thp
psi2:Apns
psi:Apns
phi:Apns
psi:Mta
phi:Mta
psi:iQoa
-180 -120 -60 0 60 120 180

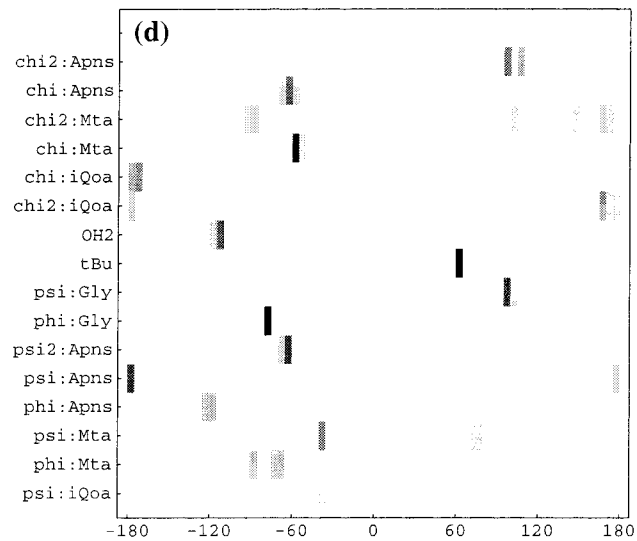
(d)
chi2:Apns
chi:Apns
chi2:Mta
chi:Mta
chi:iQoa
chi2:iQoa
OH2
tBu
psi:Gly
phi:Gly
psi2:Apns
psi:Apns
phi:Apns
psi:Mta
phi:Mta
psi:iQoa
-180 -120 -60 0 60 120 180

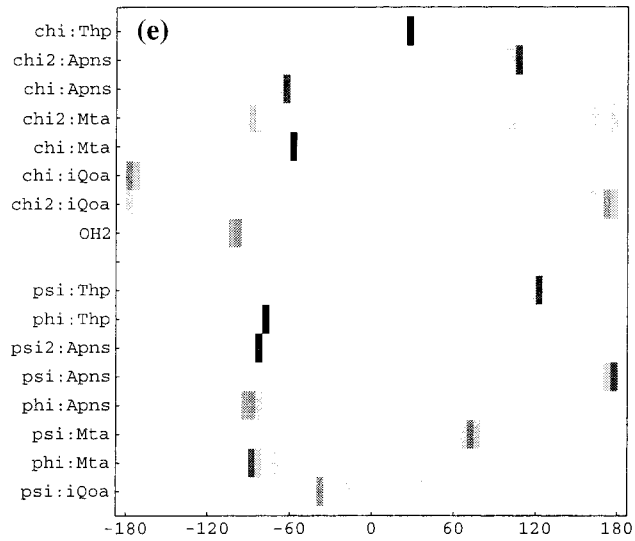
(e)
chi:Thp
chi2:Apns
chi:Apns
chi2:Mta
chi:Mta
chi:iQoa
chi2:iQoa
OH2
psi:Thp
phi:Thp
psi2:Apns
psi:Apns
phi:Apns
psi:Mta
phi:Mta
psi:iQoa
-180 -120 -60 0 60 120 180

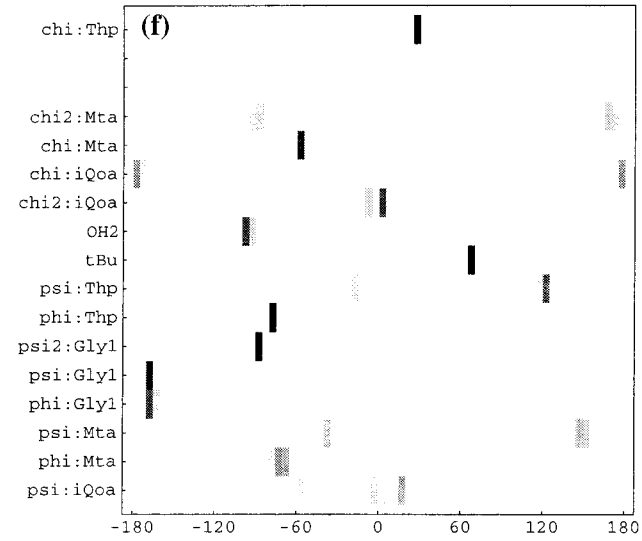
(f)
chi:Thp
chi2:Mta
chi:Mta
chi:iQoa
chi2:iQoa
OH2
tBu
psi:Thp
phi:Thp
psi2:Gly1
psi:Gly1
phi:Gly1
psi:Mta
phi:Mta
psi:iQoa
-180 -120 -60 0 60 120 180

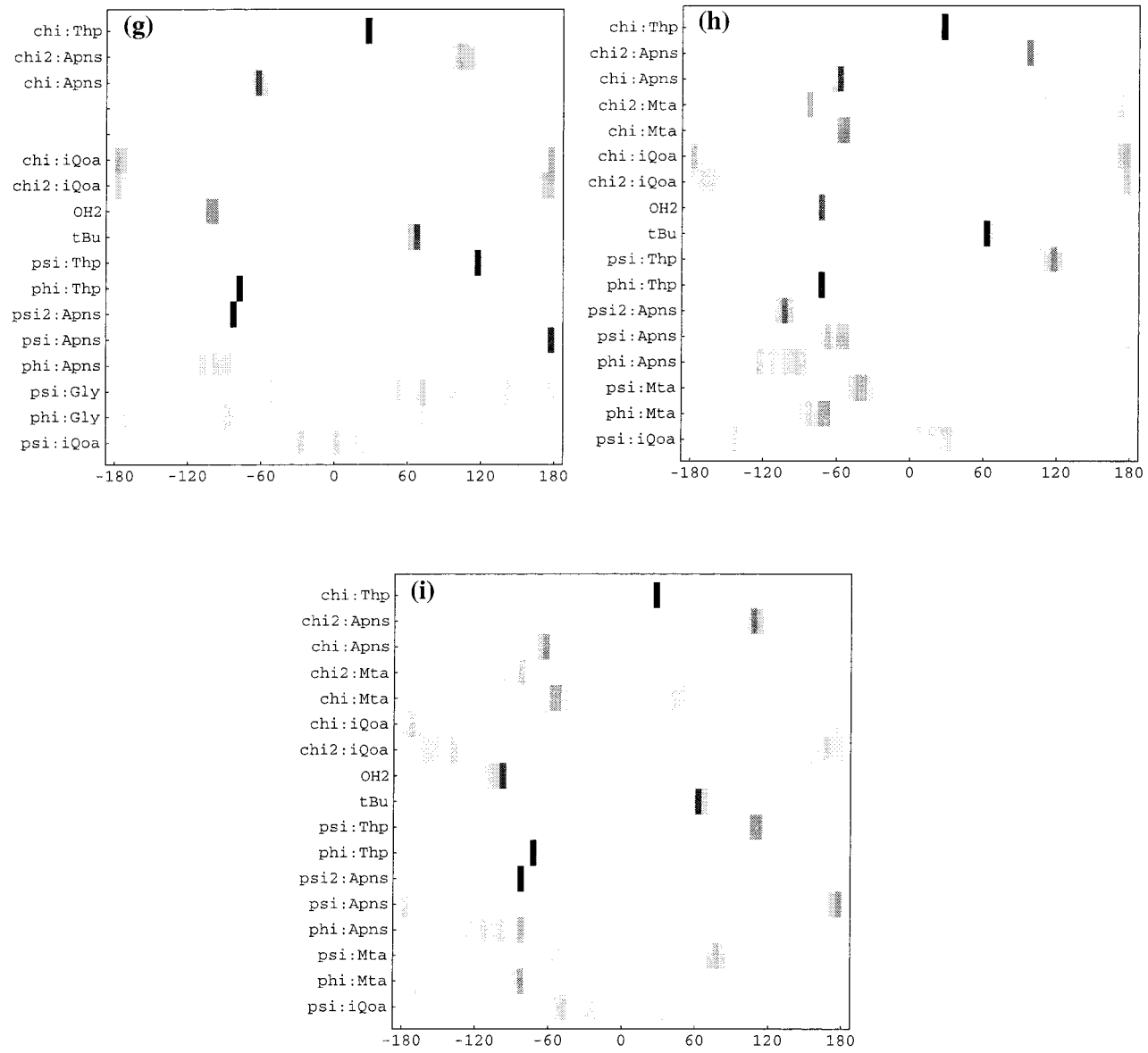

Figure 6. Computed dihedral distribution for: (a) KNI-272 in DMSO; (b) KNI-272 in DMSO, recomputed with a different initial conformation (see text); (c) KNI-272 in water; (d) KNI-272 in DMSO with Thp → Gly; (e) KNI-272 in DMSO with *t*-Bu → CH_3; (f) KNI-272 in DMSO with the Apns side chain replaced by a hydrogen; (g) KNI-272 in DMSO with Mta → Gly; (h) KNI-272 in DMSO with the charges of Apns, Thp, and *t*-Bu artificially set to 0; (i) KNI-272 in a vacuum.

TABLE 5: Summary of Computed Conformational Changes in the C-Terminal Residues of KNI-272 (Apns, Thp, *t*-Bu) due to Changes in Structure or Environment[a]

change	angle	initial value	after change
Thp → Gly	ψ_{Thp}	120°	120° (98%) and gauche$^-$ (2%)
	ϕ_{Thp}	gauche$^-$	gauche$^-$ (96%) and gauche$^+$ (4%)
t-Bu → CH3	no change		
Apns → Gly1	ϕ_{Apns}	−90°	trans
	ψ_{Thp}	120°	120° (86%) and cis (14%)
Mta → Gly	no change		
Apns−Thp−*t*-Bu neutral	ψ_{Apns}	trans	trans(9%) gauche$^-$ (91%)
water	no change		
vacuum	no change		

[a] Percentages are based upon Boltzmann averages from the mining minima calculations.

illustrated in Figure 6e, is virtually unchanged relative to KNI-272. This argues against an important preorganizing role for the *t*-Bu group.

Apns → "Gly". The central Apns residue also is relatively large, and it has the potential to interact with both the iQoa and the *t*-Bu groups. Thus, it might be expected to help preorganize KNI-272. To test this hypothesis, the side chain of this residue was replaced by a hydrogen atom. However, the extra hydroxymethyl group between the Cα and the carbonyl group of this residue was retained. The resulting residue is here termed "Gly1" because it is similar to glycine. This substitution produces significant changes in the conformation and increases the overall flexibility of the molecule (Figure 6f). The most significant change in the preorganized C-terminus is that ϕ_{Gly1}

adopts a trans form, rather than the value of about −90° found for the corresponding angle in KNI-272. This change is consistent with the fact that the trans form of ϕ is much more readily adopted by glycine than by other amino acids. Although ψ_{Thp} primarily remains in its original value of 120°, this dihedral angle now also adopts a roughly cis conformation with 14% probability. It is also of interest that the χ_2 value of the iQoa residue changes significantly when Apns is replaced by Gly1. In summary, the Apns side chain contributes significantly to the preorganization of KNI-272.

Mta → Gly. The consequences on the dihedral angle distributions of replacing Mta by Gly are illustrated in Figure 6g. The only significant change is that the two main-chain angles of the Gly residue are more broadly distributed than those for the original Mta. The C-terminal Apns−Thp−*t*-Bu residues remain preorganized.

Summary of Analogue Studies. The results of this analysis are summarized in Table 5. Of the changes examined here, the only one that significantly influences the preorganization of the C-terminal residues of KNI-272 is the replacement of the Apns side chain by a hydrogen. This allows the main-chain ϕ angle at this residue to adopt a trans conformation, due to removal of a steric clash. Interestingly, the proline-like side chain of the Thp residue is not required for preorganization.

3.2.2. Influence of Electrostatic Interactions and Solvation. The contribution of electrostatic interactions to preorganization was examined by repeating the conformational analysis of KNI-272 with the atomic charges of the C-terminal residues (Apns, Thp, *t*-Bu) set to 0. The resulting distribution of dihedral angles is illustrated in Figure 6h. In general, the distributions tend to be somewhat broader than those in KNI-272 proper (Figure 6a); this is particularly noticeable for ψ_{Thp} and $\psi_{2,Apns}$. However, the only major change is that ψ_{Apns} goes from predominantly trans to predominantly gauche$^-$. Thus, electrostatic interactions play a role in preorganizing KNI-272 for binding, because Apns is part of the preorganized C-terminus.

As discussed in the first part of the Results and Discussion, the conformational distribution of KNI-272 is not changed significantly when the dielectric constant of the solvent is changed from 45 to 80 in order to simulate water instead of DMSO (Figure 6c). It is also of interest to examine the consequences of removing the solvent entirely, because KNI-272 is largely desolvated when it is bound to HIV-1 PR. Removing solvent means setting the dielectric constant to 1 for all electrostatic interactions. The resulting conformational distribution is diagrammed in Figure 6i. This shows significant changes in some side-chain dihedral distributions and also in the N-terminal part of the main chain, ψ_{Mta}, ϕ_{Mta}, and ψ_{iQoa}. However, the main chain of the C-terminal residues Apns, Thp and *t*-Bu remains unchanged. This suggests that the forces that preorganize the C-terminus are relatively independent of the environment of KNI-272. These forces are therefore likely to operate not only in solution but also in the binding site of HIV-1 PR.

3.2.3. Preorganization of a Small-Molecule "Fragment" of KNI-272. Two angles, ψ_{Thp} and $\psi_{2,Apns}$, remain essentially fixed in KNI-272 despite changes in the molecule and in the electrostatic and solvation models considered above. Here, the basis for the preorganization of these angles is examined further by study of a small-molecule analogue of a relevant fragment of KNI-272. This molecule, illustrated in Figure 1b, was first examined in a previous computational study of KNI-272.[7]

An initial conformational analysis of this molecule with MM/GB and a solvent dielectric constant appropriate to DMSO yields distributions of ψ_{Thp} and $\psi_{2,Apns}$ very similar to those found for the full KNI-272 molecule. Thus, ψ_{Thp} is 120° with 97% probability and −10° with 3% probability and $\psi_{2,Apns}$ is essentially fixed at −80°, as in KNI-272. Repeating this calculation with the alternate set of bonds and angles (see Methods) yields the same predominant conformations for these angles. There is, however, a small increase in flexibility; ψ_{Thp} now assumes a value of −120° with a probability of 3.5%, and $\psi_{2,Apns}$ assumes a value of −160° with a probability of 9%. Overall, these results suggest that the main chain of this small-molecule analogue adopts the same conformation as the corresponding portion of KNI-272.

We hypothesized that interactions between the Apns hydroxyl and its adjacent carbonyl (C_{17}═O_4 in Figure 1b) might be important in stabilizing $\psi_{2,Apns}$ in its predominant value of −80°. This would be consistent with the tendency of the hydroxyl hydrogen to point toward the carbonyl oxygen, with a hydroxyl dihedral angle of ∼−90°. This hypothesis was tested by setting the charges of the carbonyl oxygen and carbon to 0 and 0.05 e, respectively. This deletes the dipole moment of the carbonyl while preserving the net charge of the molecule. The MM/GB calculations were then repeated. For the original set of bonds and angles, the predominant value of $\psi_{2,Apns}$ now changes to −170° with a probability of 79%, with a 21% probability of remaining near the original value of −80°. The ψ_{Thp} angle also changes somewhat; it now lies at −10° with 35% probability and adopts its normal value of 120° with only 65% probability. Very similar results are obtained when these calculations are repeated with the alternate set of bonds and angles, but the loss of preorganization becomes greater by 15−30%.

The idea that neutralizing the carbonyl of Apns reduces the preorganization of angles $\psi_{2,Apns}$ and ψ_{Thp} contrasts with the observation that turning off all charges in the C-terminal residues of KNI-272 does not cause these two angles to vary (see above). These two observations taken together suggest that these angles are preorganized in KNI-272 not only by local electrostatic interactions but also by interactions with other parts of the molecule, as discussed in the following section.

The forces organizing ψ_{Thp} were further examined by plotting the various energy terms as a function of ψ_{Thp}. Parts a and b of Figure 7 present these results for the small molecules with and without a charged carbonyl group (see above). (Here, $\psi_{2,Apns}$ and χ_{OH} are fixed in their preferred values of −86° and −90°, respectively.) It is evident from the figures that the value ψ_{Thp} is determined primarily by van der Waals and dihedral energy terms. These forces establish two local energy minima, one at about 120° and the other at −10° (350°). The relative stability of these two minima is then determined by electrostatic interactions. The minimum at 120° is favored by 7.1 kJ/mol when all charges are included, but neutralizing the carbonyl (see above) causes the minimum at −10° to be weakly favored by 1.7 kJ/mol.

3.2.4. Strain in the Norstatine−Thioproline Linkage. The previous ab initio quantum mechanical analysis of KNI-272[7] concluded that the norstatine−thioproline dihedral angle, here termed ψ_{Thp}, is not in its lowest-energy position when KNI-272 is bound to HIV-1 PR (1hpx). Thus, the ab initio calculations on the small molecule discussed above (Figure 1b) suggested that the optimal value of this angle is about 60°. (This corresponds to 180° in the convention used previously.[7]) Twisting this angle to match the value found in the complex, 147°, was estimated to cost 8−13 kJ/mol, an energy penalty that would tend to oppose binding. In contrast, our calculations for KNI-272 consistently indicate that ψ_{Thp} prefers a value of

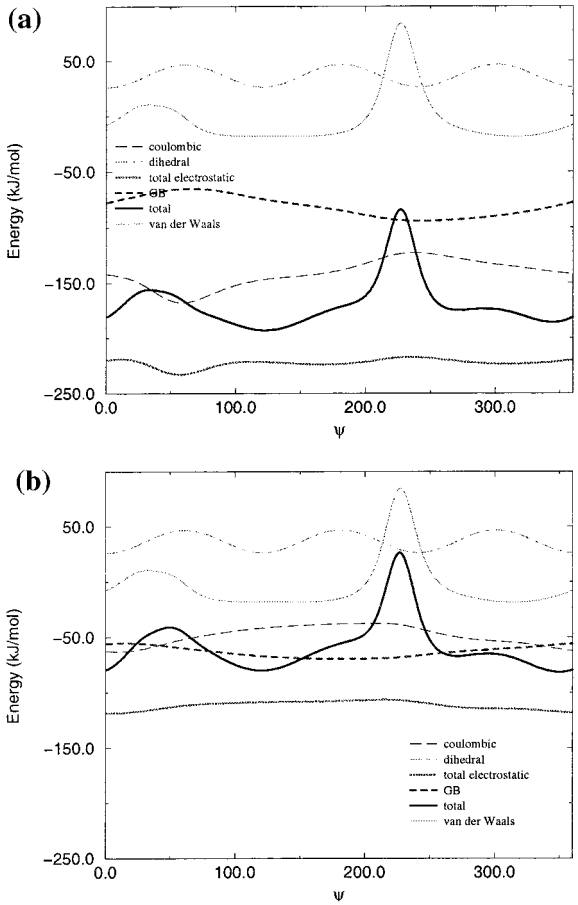

Figure 7. Computed energy (kJ/mol) of compound 4 versus ψ_{Thp} (deg) (a), and with the carbonyl group artificially neutralized (b).

118°. This is close to the value found in the complex with HIV-1 PR and in conformations A and C from the NMR study.[6]

One likely reason for the difference between our results and those of the prior ab initio study is that the latter focuses entirely on small-molecule models but the complete KNI-272 molecule may have additional interactions that change the energetics of the ψ_{Thp} rotation. In particular, artificially setting ψ_{Thp} in the crystal conformation of KNI-272 from 1hpx to the ab initio value of 60° creates a steric clash between the Apns and *t*-Bu side chains. Relaxation of this clash would require changing other dihedrals to disfavored values.

We confirmed this idea by using the mining minima method to compute the free energy difference between KNI-272 with ψ_{Thp} frozen at either 60° or 118°, but with sampling over the other 14 rotatable bonds (see the Molecular Models part of the Methods). Initial structures were generated by restraining ψ_{Thp} to 60° or 118° and then relaxing all other degrees of freedom with 1000 steps of BFGS energy minimization. The mining minima calculations indicate that KNI-272 is more stable by 18.7 kJ/mol when $\psi_{Thp} = 118°$ than when $\psi_{Thp} = 60°$. This free energy difference is attributable to the fact that the deepest energy minimum found with $\psi_{Thp} = 118°$ is 18.4 kJ/mol below the deepest energy minimum found with $\psi_{Thp} = 60°$. This analysis supports the idea that steric interactions among the bulky groups of KNI-272 contribute substantially to its preorganization. The significance of steric interactions in KNI-272 is highlighted by the space-filling model shown in Figure 8.

It is worth discussing the fact that our calculations for the small-molecule fragment (Figure 1b) do not yield the value of ψ_{Thp} found to be most stable in the prior ab initio study. This difference could result from a difference between the CHARMM energy function and the ab initio energy surface. Alternatively, it could result from our treating bonds and angles as rigid. In any case, this disagreement for the small molecule does not invalidate our conclusions regarding the importance of steric interactions in KNI-272 as a whole.

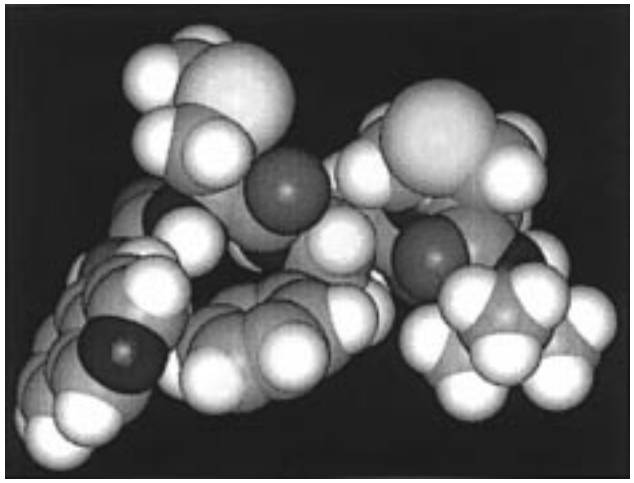

Figure 8. Space-filling illustration of KNI-272.

3.3. Comparison of Calculated Results with Experiment. As described in the Methods, the NMR study yielded a collection of interproton distances and coupling constants appropriate to the trans form of KNI-272. These data were used to generate three trans solution conformations of KNI-272, designated A, B, and C. Further study provided information on the relative populations of the trans and cis forms of the Thp amide. The following subsections compare conformations A, B, and C with the conformations represented by clusters C1, C2, and C3 from our calculations. Then a more direct comparison with experiment is made by comparing computed interproton distances with those from the NMR study. Finally, the computed trans/cis ratio of the Thp residue is compared with experiment.

3.3.1. Calculation versus Experiment: Conformations. Table 3 gives the RMS deviations of conformations A, B, and C from the lowest-energy conformations in clusters C1, C2, and C3. Results are given for the main-chain atoms and for all the preorganized C-terminal atoms. This comparison shows that conformation A is similar to C1, with RMSD values of 0.6 Å for the main-chain and 0.4 Å for all C-terminal atoms. Both conformations also are similar to the crystal conformation of the complex with HIV-1 PR. Conformations B and C deviate from conformations C1 and C2 by 1.6−2.4 Å (main-chain atoms). However, Ohno and co-workers provide evidence suggesting that their conformation A is more probable than conformations B and C.

Table 4 allows a comparison of the mean dihedrals for clusters C1, C2, and C3 with the dihedrals of conformations A, B, and C. The similarity of conformation A with cluster C1 is evident; the mean values of all but two dihedral angles for C1 are within 20° of the dihedrals of conformation A. The two deviant angles, ψ_{iQoa} and ϕ_{Mta}, are in the relatively flexible N-terminus of KNI-272.

A comparison of conformations B and C with C2 and C3 shows two major differences (Table 4). First, ψ_{Mta} is fixed in a gauche$^+$ conformation in the NMR conformations, but in the calculations, this angle can be gauche$^+$, gauche$^-$, or trans. Conversely, ψ_{Apns} is fixed in a trans conformation in the calculations but adopts all three possible conformations in the three NMR structures.

TABLE 6: Comparison of Interproton Distances (Å) in KNI-272 with Those Inferred from NOE Data (Ref 6)[a]

	NMR				calculated					
proton pair	mean	C.A	C.B	C.C	mean	C.1	C.2	C.3	NOE	CX
QoaCα−MtaNH	2.59	2.81	2.35	2.80	3.1	3.11	3.23	3.29	≤3.5	3.1
iQoaCα−ApnsCϵ	3.14	3.06	3.15	3.22	3.8	3.12	**7.38**	**9.29**	≤4.5	2.6
iQoaCα−ApnsNH	**4.71**	**4.70**	**4.89**	**4.58**	**4.2**	**4.26**	**6.29**	**4.26**	≤3.5	**4.3**
MtaNH−MtaCβ	3.13	3.15	3.11	3.13	2.7	2.66	2.76	2.76	≤3.5	2.9
MtaNH−ApnsNH	3.34	3.36	3.43	3.26	2.7	**3.70**	**4.60**	2.40	≤3.5	3.5
MtaNH−ApnsCϵ	4.20	4.14	4.14	4.36	*5.5*	*5.41*	*7.73*	*6.17*	≤4.5	4.1
MtaCα−ApnsNH	2.19	2.26	2.11	2.23	2.5	2.30	2.20	**3.40**	≤2.5	2.4
MtaCα−MtaCδ	4.38	4.39	4.35	4.41	3.4	**4.86**	2.82	**4.96**	≤4.5	2.5
MtaCβ−MtaCδ	2.92	2.92	2.92	2.93	3.0	2.97	3.09	2.91	≤4.5	3.0
MtaCβ−ApnsCδ	**6.44**	**6.48**	**6.40**	**6.45**	3.8	**6.85**	**5.91**	3.46	≤4.5	**6.4**
MtaCδ−ApnsCϵ	*7.10*	*7.09*	*7.01*	*7.20*	*5.2*	*10.02*	*7.29*	4.49	≤4.5	*8.8*
ApnsNH−MtaCβ	4.28	4.32	4.20	4.33	3.1	4.39	2.86	2.87	≤4.5	**4.6**
ApnsNH−ApnsCβ	**2.75**	**2.74**	**2.88**	**2.67**	**2.8**	**2.66**	**2.66**	**2.86**	≤2.5	**2.9**
ApnsNH−ApnsCβ$_2$	2.95	2.88	**3.77**	2.73	3.2	3.30	3.40	3.20	≤3.5	3.0
ApnsNH−ApnsCδ	3.78	3.70	3.84	3.81	3.1	3.12	3.01	3.12	≤4.5	3.1
ApnsNH−MtaCδ	**6.11**	**6.16**	**6.08**	**6.10**	**5.4**	**6.98**	4.09	**5.38**	≤4.5	**4.8**
ApnsCα−ApnsCδ	2.61	2.74	2.61	2.51	2.9	2.90	3.00	3.10	≤4.5	3.0
ApnsCα−ApnsCϵ	*4.86*	*4.88*	*4.87*	*4.83*	*5.0*	*4.96*	*5.04*	*5.12*	≤4.5	*5.1*
ApnsCα−ThpCδ	2.94	2.48	**4.15**	**4.39**	2.3	2.34	2.34	2.34	≤3.5	2.4
ApnsCβ−ApnsOH	3.21	2.83	**4.45**	3.36	2.9	2.92	2.85	2.88	≤3.5	2.3
ApnsCβ−ApnsCβ$_2$	3.06	**3.79**	2.95	2.86	**3.8**	**3.80**	**3.85**	**3.80**	≤3.5	**3.8**
ApnsCβ−ApnsCδ	2.74	2.72	2.74	2.75	3.0	2.75	2.75	2.71	≤4.5	2.7
ApnsCβ−ApnsCϵ	*4.99*	*4.99*	*4.99*	*5.00*	*5.0*	*4.98*	*5.02*	*4.98*	≤4.5	*5.0*
ApnsCβ2−ThpCδ	2.31	2.30	2.40	2.25	2.3	2.28	2.28	2.28	≤3.5	2.2
ApnsCδ−*t*-BuCβ	3.71	**4.71**	3.14	**6.81**	3.9	3.89	3.76	3.89	≤4.5	4.5
ApnsCϵ−*t*-BuCβ	*6.12*	*6.36*	*5.45*	*8.07*	*5.9*	*5.70*	*5.84*	*5.96*	≤4.5	*6.6*
ThpCβ−ThpCδ	3.67	3.61	3.70	3.71	3.9	3.88	3.88	3.88	≤4.5	4.0
Violations	8	10	11	10	9	12	11	11		10

[a] Protons are identified via the heavy atoms to which they are bonded. NMR: distances computed for the NMR structures C.A, C.B, and C.C,[6] and also averaged over all three structures with eq 6 (mean). Calculated: distances computed for lowest-energy conformation in each cluster, C.1, C.2, and C.3, and also computed as a Boltzmann-weighted average over the entire set of conformations (mean). NOE: distances inferred from the NMR study.[6] CX: distances computed from the crystal conformation with HIV-1 PR.[3] Distances in bold or *italic* type disagree with the NOE-derived distance. Violations in italic type are those involving the Cϵ hydrogens of Apns (see text). Violations: total number of NOE distance violations (bold and italic).

3.3.2. Calculation versus Experiment: Interproton Distances. Comparing our calculated structures with conformations A, B, and C from the experimental study is an indirect way of comparing calculation with experiment. This is because the NMR conformations are not primary data. Rather, they are models generated with molecular dynamics simulations and intended to maximize the fit to the underlying experimental data. This section describes a more direct comparison between calculation and experiment, in which computed average interproton distances (Methods, subsection 2.3.2) are compared with the distances considered by Ohno and co-workers to be consistent with their measurements (see Methods, subsection 2.1). Distances were calculated as Boltzmann averages over all conformations and also for the lowest-energy representative of clusters C1, C2, and C3. For comparison, distances were also computed for conformations A, B, and C from the NMR study. Average distances also were computed from conformations A, B, and C with the assumption that the three conformations are equally probable in solution. (Note, however, that Ohno and co-workers suggest that conformation A is the most probable.) Finally, distances were computed for the crystal conformation of KNI-272 complexed with HIV-1 PR (1hpx). The results are given in Table 6, along with the distances predicted directly from the NOE measurements. Distances that violate the NOE-derived distances are in either bold or italic type, where italic indicates a violation involving the hydrogens of Apns Cϵ (see below). The table also lists the number of violations in each set.

A striking overall result is that the number of NOE violations (9) for our computed conformational distribution is slightly smaller than the number of violations for conformations A (10), B (11), or C (10). This is despite the fact that conformations A, B, and C were derived with experimental constraints, while our conformational distribution did not rely upon experiment. Simple averaging over conformations A, B, and C reduces the number of violations, but the final count of eight is only slightly better than the computational result of nine violations. The experimentally derived structures show two NOE violations that are particularly marked: Mta Cβ−Apns Cδ and Mta Cδ−Apns Cϵ. The only conformation in Table 6 for which the distances match experiment is C3. This is traceable to the value of ψ_{Mta}; C3 is the only conformation with a value of −40° for this angle. This suggests that ψ_{Mta} spends a significant fraction of time near the C3 value of −40°.

The nine NOE violations found in our global average are now discussed. First, the NOE between the protons of Apns Cβ and Apns Cϵ is inherently difficult to interpret. The strength of the NOE suggests an interproton distance of ≤4.5 Å, but this seems to be inconsistent with the range of energetically feasible conformations. The distance between the Apns Cβ and Apns Cϵ protons are controlled by one dihedral, $\chi_{2,Apns}$. Changing this angle from 0 to 360° causes the interproton distance to range between 4.6 and 5.5 Å. It is therefore unlikely that the mean interproton distance is actually ≤4.5 Å, and indeed, this constraint is not satisfied in conformations A, B, and C from the NMR study either (see Table 6). This analysis suggests that the distance constraints derived from the NMR study should not be viewed as absolute.

Four of the remaining differences between computation and experiment are also associated with the hydrogens of Apns Cϵ.

These distances are therefore influenced by $\chi_{2,Apns}$. The calculations yield values in the range 90−110° for this angle, but changing it by only about 30° would yield agreement with the NOE-derived distances for three of these four interproton distances: Apns Cα−Apns Cϵ, Mta Cδ−Apns Cϵ, and Apns Cϵ−*t*-Bu Cβ. It is perhaps worth noting that this angle adopts a value of 100.5° in the complex of KNI-272 with HIV-1 PR, consistent with our calculations but not with the NMR study. In summary, the results we obtain for these three interproton distances do not differ markedly from experiment, and they are listed in italic type, rather than bold type, in Table 6.

The fourth interproton distance involving Apns Cϵ is Mta NH−Apns Cϵ. This is not corrected by adjusting $\chi_{2,Apns}$. Rather, the difference between calculation and experiment is best attributed to an error in the value of ϕ_{Mta} from the calculations. The calculations yield values of roughly −70°, while the NMR refinement yielded a value of −145° for this angle and thereby good agreement with the experiment NOE. Thus, the calculations and the NMR study appear to differ significantly in this regard, and the wrong results are noted in bold type in Table 6. In the crystal conformation, ϕ_{Mta} equals −119°; this lies between the calculated and NMR values but is slightly closer to the NMR values.

The computed interproton distance for Mta Cδ and Apns Cϵ, 5.2 Å, also deviates from the experimental result, ≤4.5 Å. However, this distance is strongly influenced by the conformation of the flexible Mta side chain, so the deviation does not imply an important error in the overall conformation of KNI-272.

Three more differences between computational and experimental interproton distances remain to be discussed. These are $C\alpha_{iQoa}-NH_{Apns}$, Apns NH−Apns Cβ, and Apns Cβ−Apns Cβ_2. In each case, the NMR conformation deemed most probable, CA, also violates the NOE distances. However, conformations B and C satisfy the distance restraint for Apns Cβ−Apns Cβ_2. It is not clear why both the NMR analysis and our theoretical analysis disagree with experiment in these instances.

3.3.3. Calculation versus Experiment: Trans/cis Amide Ratio. The analysis so far has focused on conformations of KNI-272 in which the Apns−Thp amide bond is trans. Indeed, the NMR study of Ohno and co-workers demonstrated that the trans form of this bond is more highly populated than the cis form, with a trans/cis ratio of 5.6. Moreover, when KNI-272 binds to HIV-1 PR, this amide bond is fixed in the trans conformation, consistent with the selectivity of HIV-1 PR for the trans conformation of the Tyr−Pro amide bond in the p17/p24 cleavage site of the Gag polyprotein substrate.[26] Thus, the conformation of this amide bond is critical to the action of KNI-272 at HIV-1 PR, and it is of interest to learn whether the present computational approach can reproduce the experimentally determined tendency to adopt the trans conformation.

We computed the trans/cis ratio by using the mining minima method to determine the free energy difference between KNI-272 in the trans and the cis conformations, with a solvent dielectric constant appropriate to DMSO (45), as described in the Methods. The free energy difference is 4.4 kJ/mol, favoring the trans conformation. This corresponds to a trans/cis ratio of 6.0 at the experimental temperature of 293 K, which agrees very well with the measured ratio of 5.6.[6]

Murcko and co-workers[7] also examined the conformational preference of this amide bond by studying small model compounds with ab initio quantum mechanics calculations. They concluded that the trans conformation is not inherently more stable than the cis conformation. They argue accordingly that the only reason KNI-272 binds HIV-1 PR in the trans conformation is to allow the C-terminal amide oxygen to receive a hydrogen bond from the flap water (301) localized in the binding site. However, their Figure 4 indicates that the trans conformation is more stable by roughly 4 kJ/mol, which is consistent with the NMR results[6] and with our calculations.

4. Conclusions

The present study has used a novel and efficient computational approach to analyze the conformational preferences of the potent HIV-1 PR inhibitor KNI-272. The calculations indicate that KNI-272 does have an intrinsic tendency to assume the active conformation found in its complex with HIV-1 PR, even when it is free in solution; that is, the inhibitor is significantly preorganized. The most rigid part appears to be the C-terminus formed by the residues Apns, Thp, and *t*-Bu. One might expect the restrictive Thp group to be important in fixing the conformation of this inhibitor, but we find that replacing the Thp residue by the maximally flexible residue glycine does not mobilize the chain significantly. However, steric interactions among the bulky side chains and terminal groups do appear to be important in preorganizing KNI-272. In particular, steric interactions involving the Apns groups appear to be important in fixing the norstatine−carboxamide torsion angle. Artificially deleting atomic charges allows the conformational distribution to shift. However, adjusting the dielectric constant of the solvent in a physically reasonable range does not destroy the preorganization of KNI-272.

In summary, although one might expect this peptide-like inhibitor to be extremely flexible, it appears to have an intrinsic tendency to assume its bioactive conformation. That is, it is preorganized, as previously argued.[3,6] The forces that lead to its preorganization, covalent bonding, steric interactions, and electrostatics, are expected to be operative not only in solution but also in the binding site of HIV-1 PR. They should thus contribute to the observed potency of this inhibitor.

The present study also presents a detailed comparison of computation versus experiment. The agreement between the calculated conformational distribution of KNI-272 and the NMR data justify the use of the present computational method. Thus, the mean interproton distances that we compute theoretically agree with the measured NOEs as well as those of conformations previously generated using the NOE-derived distances as restraints.[6] The differences between our computations and experiment seem best accounted for by a significant error in the computed value of ϕ_{Mta}, and by a minor error in $\chi_{2,Apns}$. In addition, the computed free energy difference between the trans and cis forms of KNI-272 agrees with the ratio measured by NMR. The present methodology should be useful in analyzing the conformational preferences of other molecules as well; further validation studies will be of interest.

Acknowledgment. This work was supported by the National Institutes of Health (GM54053 to M.K.G.) and the National Institute of Standards and Technology. M.S.H. was supported by a National Research Council Research Associateship. Certain commercial equipment or materials are identified in this paper in order to specify the methods adequately. Such identification does not imply recommendation or endorsement by the National Institute of Standards and Technology, nor does it imply that the materials or equipment identified are necessarily the best available for the purpose.

References and Notes

(1) Kiso, Y. *Biopolymers* **1996**, *40*, 235.
(2) Kageyama, S.; Mimoto, T.; Murakawa, Y.; Nomizu, M.; Ford, H., Jr.; Shirasaka, T.; Gulnik, S.; Erickson, J.; Takada, K.; Broder, S.; Kiso, Y.; Mitsuya, H. *Antimicrob. Agents Chemother.* **1993**, *37*, 810.
(3) Baldwin, E. T.; Bhat, T. N.; Gulnik, S.; Liu, B.; Topol, I. A.; Kiso, Y.; Mimoto, T.; Mitsuya, H.; Erickson, J. W. *Structure* **1995**, *3*, 581−590.
(4) Dyson, H. J.; Merutka, G.; Waltho, J. P.; Lerner R. A.; Wright, P. E. *J. Mol. Biol.* **1992**, *226*, 795.
(5) Dyson, H. J.; Sayre, J. R.; Merutka, G.; Shin, H.-C.; Lerner R. A.; Wright, P. E.; *J. Mol. Biol.* **1992**, *226*, 819.
(6) Ohno, Y.; Kiso, Y.; Kobayashi, Y. *Bioorg. Med. Chem.* **1996**, *4*, 1565.
(7) Murcko, M. A.; Govinda Rao, B.; Gomperts, R. *J. Comput. Chem.* **1997**, *18*, 1151.
(8) Head, M. S.; Given, J. A.; Gilson, M. K. *J. Phys. Chem.* **1997**, *101*, 1609.
(9) Luo, R.; Head, M. S.; Moult, J.; Gilson, M. K. *J. Am. Chem. Soc.* **1998**, *120*, 6138.
(10) Luo, R.; David, L.; Hung, H.; Devaney, J.; Gilson, M. K. *J. Phys. Chem.*, in press.
(11) Luo, R.; Head, M. S.; Given, J. A.; Gilson, M. K. *Biophys. Chem.*, in press.
(12) Wuthrich, K. *NMR of Proteins and Nucleic Acids*; J. Wiley: New York, 1986; pp 177−182.
(13) Creighton, T. E. *Proteins. Structures and Molecular Properties*, 2nd ed.; W. H. Freeman and Co.: New York, 1993; p 5.
(14) Davis, M. E.; Madura, J. D.; Luty, B. A.; McCammon, J. A.*Comput. Phys. Comm.* **1991**, *62*, 187.
(15) Gilson, M. K.; Given, J. A.; Head, M. S.; Bush, B. L.; McCammon, A. *Biophys. J.* **1997**, *72*, 1047.
(16) Brooks, B. R.; Bruccoleri, R. E.; Olafson, B. D.; States, D. J.; Swaminanathan, S.; Karplus, M. *J. Comput. Chem.* **1983**, *4*, 187.
(17) Clark Still, W.; Tempczyk, A.; Hawley, R. C.; Hendrickson, T. *J. Am. Chem. Soc.* **1990**, *112*, 6127.
(18) Sitkoff, D.; Sharp, K. A.; Honig, B. *J. Phys. Chem.* **1994**, *98*, 1978.
(19) Qiu, D.; Shenkin, P. S.; Hollinger, F. P.; Clark Still, W. *J. Phys. Chem. A* **1997**, *16*, 3005.
(20) Sitkoff, D.; Sharp K. A.; Honig. B. *J. Phys. Chem.* **1994**, *98*, 1978.
(21) Mohamadi, F.; Richards, N. G. J.; Guida, W. C.; Liskamp, R.; Lipton, M.; Caufield, C.; Chang, G.; Hendrickson, T.; Still, W. C. *J. Comput. Chem.* **1990**, *11*, 440.
(22) Sridharan, S.; Nicholls, A.; Honig, B. *FASEB J.* **1992**, *6*, A174.
(23) Molecular Simulation, Inc., Waltham, MA.
(24) Press, W. H.; Teukolsky, S. A.; Vetterling, W. T.; Flannery, B. P. *Numerical Recipes in Fortran 77*, 2nd ed.; Cambridge University Press: Cambridge, 1996.
(25) Kabsch, W. *Acta Crystallogr.* **1978**, *A34*, 827.
(26) Vance, J. E.; Leblanc, D. A.; Wingfield, P.; London, R. E. *J. Biol. Chem.* **1997**, *272*, 15603.